Enhancement in Swimming Speed Leads to a More Efficient Chemotactic Response to Repellent

Richa Karmakar[1], R.V.S. Uday Bhaskar[1], Rajesh E Jesudasan, Mahesh S. Tirumkudulu, K. V. Venkatesh

Department of Chemical Engineering, Indian Institute of Technology Bombay, Mumbai 400076

Correspondence:

K. V. Venkatesh,
Department of Chemical Engineering, Indian Institute of Technology Bombay,
Mumbai - 400076, India
Fax:+91 (22) 2572 6895, Tel:+91 (22) 2576 7223, Email: venks@iitb.ac.in

Mahesh S. Tirumkudulu,
Department of Chemical Engineering, Indian Institute of Technology Bombay, Mumbai - 400076, India
Fax:+91 (22) 2572 6895,
Tel:+91 (22) 2576 7227,
Email: mahesh@che.iitb.ac.in

1RVSU and RK have equally contributed to the work.

Abstract

Negative chemotaxis refers to the motion of microorganisms away from regions of high concentration of chemorepellents. In this study, we set controlled gradients of $NiCl_2$, a chemorepellent, in microchannels to quantify the motion of *Escherichia coli* over a broad range of concentrations. The experimental technique yielded the motion of the bacteria in space and time and further related the motion to the local concentration profile of the repellent. Results show that the swimming speed of bacteria increases with increasing concentration of repellent which in turn enhances the drift velocity. The contribution of the increased swimming speed to the total drift velocity was in the range of 20-40% with remaining contribution coming from the modulation of the tumble frequency. A simple model that incorporates receptor dynamics including adaptation, intra-cellular signaling and swimming speed variation was able to qualitatively capture the observed trend in drift velocity.

INTRODUCTION

Rod shaped bacteria, such as *Escherichia coli*, have evolved to move away from unfavorable chemicals (chemorepellents) and towards regions containing favorable chemicals (chemoattractants). This strategy of movement or taxis is well known as chemotaxis. The motion is executed with the help of helically shaped locomotive organelles present on the cell surface known as flagella. *E. coli* responds to the changing environmental conditions by alternating the rotational direction of their flagella. Counterclockwise (CCW) rotation (as viewed from the tip of the flagella toward the cell body) results in a motion called run, whereas clockwise (CW) rotation leads to the tumbling of the bacteria. By modulating the duration of runs and tumbles, the bacteria achieves a net motion towards chemoattractants or away from chemorepellents. Bacterial transmembrane chemoreceptors help in detection of chemical stimuli in the environment and thereby transmitting the signal to the cytoplasmic signal transduction system. The probability of clockwise rotation (CW) is controlled by the phosphorylation state of a chemotactic protein, CheY. When phosphorylated, the CheY binds to the switch proteins at the flagellar motor in the cytoplasm leading to increased tumble. The phosphorylation of CheY is catalyzed by a kinase, CheA, whose activity in turn is regulated by the chemoreceptors. When an attractant binds to the chemoreceptors, the activity of CheA is reduced leading to long runs. In contrast, the activity is enhanced in case of a repellent, thereby increasing the number of tumbles (1).

In this work, we focus on the response of the bacteria to the chemorepellent, $NiCl_2$. Adler and co-workers were the first to quantify the response of *E. coli* to various chemorepellents (2). Using both the agarose gel assay and the microchannel assay, they determined the threshold concentration necessary for negative chemotaxis for a range of chemicals with different chemical groups. They showed that the chemotactic response was dependent on the existence of a suitable receptor; in the absence of such receptors, the

bacteria showed no response even at high repellent concentrations. Similar studies on repellents by others have been reported for various chemicals (3). Mao et al. (4) fabricated a sensitive microfluidic device to detect the chemotactic response to both chemoattractants and repellents, such as, nickel sulfate and L-leucine. The device was demonstrated to be sensitive and robust. A microfluidic device based on similar principles capable of maintaining stable gradients was shown to be an alternative experimental protocol to characterize chemotaxis to both attractants and repellents (5). Here, the cells are introduced at one end of the microfluidic channel with cells convected by the background flow along the channel. A stable chemical gradient is set-up across the channel and the extent of chemotaxis is measured in terms of a chemotaxis partition coefficient and a chemotaxis migration coefficient. While the former quantifies the direction of migration of cells, the latter quantifies the number of cells that migrate across the channel. Khan et al. (6) analyzed repellent signal processing in *E. coli* by flash photorelease of leucine and found that the response amplitudes of free-swimming cell populations increased with a step change in leucine concentration. Further, they showed that the motor response time of individual cells correlated with rotational bias but not the cell size. It has been shown that the transmembrane receptor, Tar, is required for chemotaxis to nickel (7). Eisenbach et al. (8) have shown that the repellent response to nickel sulfate is not influenced by changing the cytoplasmic membrane fluidity. Further, they showed that the response did not change for periplasm-void cells confirming that the receptors for nickel ions are on the cytoplasmic membrane. This has been recently reconfirmed by Englert et al. (9) where they show that the Ni^{2+} ion binds specifically to the periplasmic domain of the Tar receptor but not to the periplasmic domain of the Tsr. However, the exact mechanism involved in the sensing of Ni^{2+} ions is yet to be elucidated.

While most of the studies on chemotaxis that relate the cell motility to the intra-cellular signaling pathway have focused on attractants by relating quantities such as rotational

bias and drift velocity to the attractant concentration and its gradients via the known receptor binding characteristics and signaling pathway (10-19), similar studies have not been performed for repellents. Consequently, very little is known on how repellents interact with receptors and what signals they induce in the intra-cellular pathway (20). Further, the phenotypic response to repellents, i.e., the influence of repellent concentration and gradient on the details of cell motility including swimming speed and drift velocity are unknown. In this paper, we focus on the latter by establishing controlled gradients of $NiCl_2$ in microchannels to quantify the chemotactic response in terms of drift velocity and swimming speed over a wide range of repellent concentrations. While the cells migrate away from regions of high concentration of repellents to regions of lower concentrations, detailed analysis revealed that the swimming speed of bacteria increases with increasing concentration of repellent which in turn enhances the drift velocity. The increased swimming speed was found to contribute about 20-40 % to the drift velocity with the remaining contribution from modulation of tumble frequency. Based on the existing mathematical model for attractants, we propose a simple two-state model to describe the receptor dynamics and adaptation including the variation in the swimming speed in response to repellents. This model successfully predicts the measured drift velocities and demonstrates that the increased swimming speeds play an important role in migration.

MATERIALS AND METHODS

Strain

Escherichia coli wild-type strain, RP437 and the Tar-deletion mutant, (RP2361, henceforth referred to as RP437Δ*tar*), both gifts from Professor J S Parkinson (University of Utah, USA), were used in experiments.

Media

Tryptone (casein enzymic hydrolysate 10.0, Sodium Chloride 5.0) was obtained from Merck®. The chemicals, KH_2PO_4, K_2HPO_4, $MgSO_4.7H_2O$, Ethylene-di-amine-tetra acetic acid, and Poly(vinyl)-pyrollidine were obtained from Sigma-Aldrich®. The motility buffer (MB) contained K_2HPO_4, 11.2 g; KH_2PO_4, 4.8 g; $(NH_4)_2SO_4$, 2 g; $MgSO_4$. $7H_2O$, 0.25 g; PVP, 1 g; and EDTA, 0.029 g in one litre of distilled water. Tryptone medium contained tryptone, 15 g in one litre of distilled water. The repellent, $NiCl_2$. $6H_2O$ (ultra pure), was obtained from Loba Chemie® (Mumbai, India) and was added to the motility buffer to obtain varying concentrations of repellent.

Growth conditions

A loop full of *E. coli* strain was inoculated into 50 ml of tryptone broth and was allowed to grow for 9 hr at 30ºC and 200 rpm. Once the bacterial culture reached mid-exponential phase (optical density, OD ≈ 0.8-1.0), 5-10 % of the inoculum was transferred to the same medium and grown for 3 hr to ensure adaptability to the medium. The culture was then centrifuged at 4000 rpm for 10 min and the resulting cell pellet was washed gently two times with motility buffer. About 0.02 µL of the cell pellet was used in the capillary experiments.

Experiment protocol

Growth and death experiments

Growth experiments were performed in tryptone medium with various concentrations of $NiCl_2$. The OD was measured using UV Spectroscopy at 600 *nm* at various times and the specific growth rate (µ) was obtained from the slope of logarithm of the OD verses time curve. Experiments were also performed to determine the death rate constant. Here, the cells grown in tryptone medium were resuspended in 100 *ml* of phosphate buffer solution along with various concentrations of the repellent. The viable cell count at various time points was

143 obtained using the methylene blue reduction assay (21). The slope of the logarithm of the
144 viable cell count verses time yielded the death rate constant (*K*).

145 **Measurement of cell motion**

146 Glass microchannels (RT5010) of dimensions 5 cm (L) x 1000 µm (W) x 100 µm (H)
147 obtained from Arte Glass Associates Co., Ltd., Japan were used for the chemotaxis
148 experiments. An inverted microscope (IX71, Olympus, Japan) fitted with a monochrome
149 camera (Evolution VF Cooled camera, Media Cybernetics, Japan) was used to image the
150 cells. Imaging was performed using dark-field mode of illumination with a 40X objective
151 lens (0.75 NA).

152 To observe the response of *E. coli* to different $NiCl_2$ gradients, a 4.5 cm long liquid
153 plug of low repellent concentration or motility buffer was drawn into the microchannel
154 followed by a 0.5 cm long liquid plug of higher concentration of repellent. Cells were
155 introduced into the microchannel by contacting a cell pellet with the mouth of the
156 microchannel at the higher repellent concentration end (Fig.1). The ends of the microchannel
157 were sealed with wax. The duration of the experiments varied from 15 to 40 min (the latter
158 in plain motility buffer) which ensured that the motility was robust through out the
159 experiments. Four different repellent gradients, namely, 10-0, 50-0, 100-0, and 100-90 were
160 established in the microchannel, where the first number refers to the higher repellent
161 concentration (in µM) in the 0.5 cm liquid plug and the second refers to the lower
162 concentration in the 4.5 cm liquid plug. Experiments were also performed in plain motility
163 buffer and with a uniform concentration of 100 µM of $NiCl_2$. Each experiment was repeated
164 three times on different days to capture the variability.

165 The movement of the bacteria was recorded at a distance of 500, 1000, 1500 and 2000 µm
166 from the edge of the pellet. The images were taken at frame rates of 21 fps. The trajectories
167 of the cells were obtained using a commercial software, Image Pro Plus, and the data was

further processed to obtain the swimming speed, drift velocity, and cell orientation from more than 2000 cells for each condition. The software parameters were set such that only those cells within ±1 µm of the focal plane were considered. Further, only those tracks were considered where the cell spent at least 0.5 seconds in the focal plane thereby ensuring that all out-of-plane motions were ignored by the analysis. A tumble event was identified when the swimming speed of the cell was below half the mean swimming speed, and the change in the turn angle was greater than 4º between successive frames (at 21 fps). These conditions were obtained by visual inspection of run and tumble events and are similar to those reported by Alon et al. (22). The measured average swimming speed of 18.2±7.9 µm/s (average ±s. d.) and an average turn angle of 71º for RP437 cells dispersed uniformly in a microchannel containing plain motility buffer is close to those observed for the same strain by Saragosti et al. (23) who report values of 18.8 ±8.2 µm/s and 69º, respectively. These results confirm the correctness of the methodology used in the study. For further details on image analysis, refer to Vuppula et al. (10).

The head-rotation speed was determined using a 10X objective (0.30 NA) in conjunction with a dark-field condenser. High speed imaging of the cells (400 fps using Hamamatsu ORCA flash 4.0 V2) reveals time varying light intensity fluctuation of cells caused by its rotating head. Images at a resolution of 512 × 512 pixels were recorded for approximately 12s over an area of 332 µm × 332 µm containing around 500 cells. Experiments for each condition were repeated over 10 times over three different days to obtain the average power spectrum from about 5000 cells. Following Martinez et al. (24), we divided the image into equal sized bins so that each bin contained approximately one cell, and determined the power spectrum of the intensity fluctuation of each bin. The power spectrum was then averaged over all bins to reveal the power spectrum for the entire population. Finally, the power spectrum was normalized by the square of the frequency to eliminate contribution from Brownian motion of

dead or non-motile cells and all intensity values of the power spectrum were rescaled with the maximum value. The peak value of the corrected power spectrum gives the dominant head-rotation speed of the population. The peak value was obtained by fitting the power-spectrum in the frequency range of 20-100s^{-1} using a single peak log-normal distribution. The frequency spectrum is not sharp as expected for a signal with a single frequency since the spread is caused by not only a range of head-rotation rates present in the population but also the finite number of frames used for the analysis. However, the location of the peak of the spectrum will be unaffected by these factors and is expected to give the dominant head-rotation speed of the population.

Measurement of concentration profile

The concentration profile of repellent was determined using a fluorescent technique using a 4X objective (0.13 NA) in the epifluorescence mode. In order to calibrate the intensity of varying $NiCl_2$ concentrations, a 5 cm long liquid plug of $NiCl_2$ along with 1 g/L of fluorescent indicator, Newport Green DCF, Dipotassium Salt (Invitrogen Inc), was drawn in the microchannel and the ends were sealed with wax. The fluorescent intensity (505/535 nm) of the indicator gives a quantitative measure of the concentration of Ni^{2+} ions. The fluorescence intensity was obtained for concentrations up to 500 µM (not shown). To obtain the concentration profile in gradients of repellent, a 4.5 cm long liquid plug of motility buffer were drawn into a microchannel followed by a 0.5 cm long liquid plug of 500 µM repellent concentrations. Both the liquid plugs also contained the fluorescent indicator. The evolving concentration profile was measured and it compared well with that predicted by equation (1). Note that the measurements started 2 mins after introducing the liquid plugs and the initial concentration measured at 2 min was taken as the initial condition for solving equation (1).

RESULTS

Growth and death experiments were performed in order to determine the range of repellent concentrations over which the viability is not adversely affected. Figure 2 shows the normalized specific growth rate and the death rate constants at various concentrations of $NiCl_2$. The specific growth rate shows a typical sigmoidal drop which can be characterized using the Hill equation. The strain RP437 demonstrated Hill coefficient of 0.44 and half saturation constants of 0.3 mM. The normalized death rate constant could be characterized by a power-law equation (Ae^{bC}) where, C is the concentration of the repellent. The exponent (b) was close to 0.38 μM^{-1} while the multiplicative constant (A) was about 0.22 (dimensionless). The cross-over point of profiles of the specific growth and death rates gives a quantitative measure of the harmfulness of the repellent. We find that concentrations less than 2.5 mM are conducive for growth with negligible death rates while higher concentrations are detrimental to bacteria's existence with low growth and high death rates. These results demonstrate that growth and death rates remain unaffected for concentration less than about 300 µM. Therefore, we perform experiments with a maximum concentration of 100 µM to ensure good motility of cells.

The chemotactic response of *E. coli* was characterized in terms of drift velocity, swimming speed (or run speed), and angular orientation as a function of chemotactant concentration and concentration gradients in the microchannel. In order to characterize the local repellent concentration and gradient, separate experiments were conducted using a fluorescent indicator for nickel ion concentration. The gradient was set-up using the same procedure as that for the bacterial experiments (Figure 1), wherein a liquid plug of length 0.5 cm containing repellent was brought in contact with a liquid plug containing motility buffer of length 4.5 cm inside the microchannel. The mixing of the repellent with the motility buffer resulted in a stable gradient. The fluorescent intensity was quantified in time and space under

the microscope (see Material and Methods). Figures 3(A) and (B) present the measured intensity after 2 and 25 minutes, respectively, of setting up the gradients. The measured concentration profiles were compared to the predictions obtained from the unsteady state diffusion equation for the transport of the repellent,

$$\frac{\partial C}{\partial t} = D\frac{\partial^2 C}{\partial x^2} \quad (1)$$

where the repellent concentration, $C(x,t)$ is a function of the distance from edge of the microchannel, x, and time, t, and D is the diffusivity of the repellent. The above equation was solved subject to the measured initial condition at 2 minutes, and zero flux boundary conditions at both ends of the microchannel, $\frac{\partial C}{\partial x}|_{x=0} = 0 = \frac{\partial C}{\partial x}|_{x=L}$, where $L=5$ cm is the length of the channel. The repellent concentration profiles at various times were obtained numerically. A diffusivity value of 12.5 $\times 10^{-6}$ cm^2/s was taken for the calculations (25). Figures 3(A) and (B) also contain, respectively, the initial profile and the predicted profile at 25 min obtained on solving the unsteady diffusion equation. It can be noted that the model equation was able to capture accurately the measured concentration profile thereby demonstrating the suitability of the model predictions in estimating the concentration and concentration gradient prevailing in the microchannel. It should be noted that the variation in the measured gradient is less than 6 % suggesting that the gradient is stable for the entire duration of the experiment (about 25 min). Further, the observed variation in our microchannel is similar to those observed in flow-based microfluidic devices wherein the difference in the gradient at the inlet and the outlet of the microfluidic channel is less than 10% (26).

Figure 4(A) presents the comparison of the swimming speed distributions plotted as a fraction of run events when exposed to plain motility buffer, and gradients of 10-0, 50-0 and 100-0 of $NiCl_2$ (see Material and Methods for definition of gradients). The swimming speed presented in the figure was measured at 500 µm from the edge of the bacterial pellet. A

run event is counted when a cell is in run mode between two consequent frames. The distribution in the presence of the motility buffer is narrow and peaks at about 15 µm/s with a mean value of 20.8 µm/s. While the observed distribution is similar to the motility buffer for the lowest gradient, both the peak and the average swimming speed increase for higher gradients. The peak and the mean swimming speeds for the 100-0 gradient were, 40 µm/s and 37.4 µm/s, respectively. The standard deviation in all cases was between 10 to 14 µm/s. The above results clearly indicate a shift in the swimming speed to higher values in the presence of the repellent. The significance of the difference in the average swimming speeds measured in motility buffer on one hand and the repellent on the other can be quantified by the t-test which yielded a *P* value of less than 0.0001 indicating that the differences are extremely statistically significant. Along with the standard t-test, we also performed statistical analysis using the Kruskal-Wallis rank sum test in order to determine if there are differences among the population's median swimming velocities measured in motility buffer, and gradients of 10-0, 50-0 and 100-0. Since the null hypothesis that all population are identical was rejected with *P* being much less than 0.01, a Bonferroni-Dunn post-hoc test was performed to compare individual groups. The latter performs a multiple comparison test designed to provide an upper bound on the probability that any comparison will be incorrectly found significant. The pair-wise differences were found significant at 0.05 level. The aforementioned statistical tests are identical to those performed in the past to determine differences in swimming behavior in bacterial populations (27). Figure 4(B) presents the average swimming speed as a function of cell orientation for the motility buffer and for the three gradients at 500 µm. In all the cases, the swimming speed is independent of the orientation with a mean identical to that obtained from the distribution in Fig. 4(A). The mean swimming speeds for varying concentrations of the repellent are plotted in Fig. 4(C) obtained from the gradient experiments at all four locations (500, 1000, 1500 and 2000 µm).

293 The swimming speeds increase monotonically from 22.1 µm/s to 38.8 µm/s. These results
294 show that the swimming speeds vary in response to $NiCl_2$ concentration reaching a maximum
295 speed that is 70% higher than that observed in motility buffer. The figure also includes the
296 swimming speed in plain motility buffer which is similar to that observed for the lowest
297 gradient. Figure 4 (D) presents the angular orientation of the cells for motility buffer and 50-0
298 gradient at 500 µm. Clearly, the fraction of cells oriented down the gradient is higher in case
299 of the gradient compared to that in motility buffer. It can be noted that the cell's orientation is
300 symmetric about the longitudinal axis of the channel since no gradient exists perpendicular to
301 the length of the channel.

302 Control experiments were performed with a mutant strain of RP437 lacking the Tar
303 receptor, namely, Δ*tar*, to show that the Tar receptor is involved in the increase in swimming
304 speed when cells are exposed to the repellent $NiCl_2$. Figure 5 presents the swimming
305 distribution for the mutant strain in motility buffer and in presence of repellent gradient (100-
306 0), both measured at 500 µm from the cell pellet. Clearly, the two distributions overlap
307 suggesting that sensing plays a role in the modulation of the swimming speed. The mean
308 swimming speed was about 24 µm/s (also included in Fig. 4(C)) and was invariant to the
309 repellent concentration, as expected in the absence of sensing. Note that the average
310 swimming speeds for the mutant strain at all three spatial locations for both motility buffer
311 and repellent gradient (100-0) are identical and higher by about 20% compared to that
312 obtained for the RP437 strain in motility buffer. This is expected since the mutant strain does
313 not sense the repellent. However, the reasons for the increase in the swimming speed merely
314 due to the deletion of Tar receptors are not clear, although the control experiments clearly
315 demonstrate the role of sensing in swimming speed modulation.

316 The increased swimming speed points to a faster rotational speed of the flagellar
317 motor. The motor performance can be determined either via the tethering technique or the

bead assay (28). Since the aforementioned techniques apply to single cells, they are inadequate in assessing the motor performance of a population of cells. In this respect, Martinez et al. (24) have demonstrated a high throughput method involving dark-field flicker microscopy wherein the average power spectrum of the flickering dark-field image of thousands of swimmers yields the averaged angular speed of the cell head of the population. They further showed that the head-rotation speed is linearly related to the flagellar motor performance, so that any change in the flagellar motor speed is directly reflected in the rotation speed of the head. We employed the same technique to determine the head-rotation speed for the wild-type strain and the mutant strain lacking the Tar receptor using the dark-field flicker microscopy technique for a large population of cells. Figure 6 presents the power spectrum data for both bacteria strains, RP437 and the mutant strain Δ*tar*, swimming in MB and in repellent gradient (100-0), both measured at 500 μm from the cell pellet. The lines represent fit to the data using a single peak, log-normal function. In all cases, the function was able to accurately represent the data with a coefficient of determination (R-squared value) of 0.99. The fit was used to obtain the peak value of the head-rotation speed. It should be noted that the intensity values are in arbitrary units and only the location of the peak value is relevant in determining the head-rotation speed. The power spectrum for RP437 in MB was distinct compared to that in the gradient (Fig. 6(A)). The peak intensity value occurred at 26.9±5.0 Hz and 43.2±2.1 Hz in MB and repellent gradient, respectively. This clearly demonstrates that the flagellar motor rotates faster in the gradient compared to the motility buffer. Figure 6(B) presents data for the mutant strain where the peak value and the profile overlaps for MB and the gradient. This result implies that in the mutant strain, the motor speed is unaffected in the presence of $NiCl_2$. The above results clearly suggest that the Tar sensor plays a role in enhancing the motor speed. Further, the increase in head rotation speed correlates with concomitant increase in the swimming speed.

343 Experiments were also performed at high concentrations of $NiCl_2$ but for uniform
344 concentrations (100-100) and very low gradients (100-90). Figure 7(A) presents the
345 percentage increase in swimming speed and drift velocity at different locations for 100-100
346 (uniform concentration) relative to motility buffer. The swimming speeds for the 100-100
347 case is much higher than that in motility buffer at both locations reconfirming the influence
348 of repellent on swimming speed. The increase in the drift velocity is of similar magnitude
349 suggesting that the increase is mainly due to the increase in swimming speed. However, in
350 the presence of a low gradient (but at high concentration, 100-90), the percentage increase in
351 drift velocity relative to that in motility buffer is much larger than the increase in swimming
352 speed indicating that the observed large drift velocities are due to both increase in swimming
353 speed and modulation of tumble frequency (Fig. 7(B)). Thus even a small gradient leads to a
354 significant increase in the drift velocity with the contribution of the increased swimming
355 speed to the total increase in drift velocity being about 20-25% indicating that the main
356 contribution to the drift velocity is through modulation of tumble frequency. A similar
357 analysis for gradients at lower concentrations, namely, 10-0 (Fig. 7(C)) and 100-0 (Fig.
358 7(D)), show larger increase in drift velocity compared to the swimming speed, which is in
359 line with the previous result. However, the contribution of the increase in swimming speed
360 towards the increase in drift velocity is in the range of 20-40%.

361 **Model Description**

362 While the sensing and adaptation mechanisms have been well characterized for attractants,
363 not much is known about repellents. Therefore, we adopt a simplified form of the two-state
364 model proposed by Inoue and Kaneko (29) to describe the receptor dynamics. The model
365 considers a receptor to be in two functional states, namely active and inactive, where the
366 former exhibits kinase activity. The activated receptor transmits the signal to the cytoplasmic
367 proteins of which CheA, CheB, and CheY are considered in the model. CheA

autophosphorylates which in turn phosphorylates two other regulator proteins, CheY and CheB. The phosphorylated CheY (CheY-P) activates the flagellar motor switch protein FliM causing the motor to turn clockwise thereby producing a tumble. It is known that the methylation of receptor by CheR and demethylation by CheB controls adaptation behavior of the cell in response to an attractant. However, the adaptive mechanism is not clearly understood in case of repellents. Therefore, a simple phenomenological model equation is used to capture adaptation to repellents. Equations 2 and 3 capture the dynamics of the concentration of the active receptor (T_A),

$$\frac{dT_A}{dt} = \frac{kC^n}{k_{Ni}^n + C^n} - \beta v T_A - \alpha T_A \quad (2)$$

$$\frac{dv}{dt} = \beta v T_A - \gamma v \quad (3)$$

where k, k_{Ni}, α, β, γ and n are the relevant parameters that represent the dynamics of the receptors. The active receptor concentration increases in response to repellent concentration (C) while the second and the third terms of equation (2) reduce the activity. The feedback for adaptation is provided by equation (3), wherein the dynamics of the variable v is equivalent to the demethylation process. At steady state, the concentration of the active receptors is a constant ($T_A=\gamma/\beta$) which ensures perfect adaptation to perturbations in repellent concentration.

The rate of increase of CheA-P increases with T_A and decreases with CheY and CheB concentrations (Equation (4)). Further, CheA-P phosphorylates CheY and CheB with a first order dephosphorylation (Equations (5) and (6), respectively).

$$\frac{dA_p}{dt} = k_1 T_A A - 100(A_p)Y - 10(A_p)B \quad (4)$$

$$\frac{dY_p}{dt} = 100(A_p)Y - 30(Y_p) \quad (5)$$

$$\frac{dB_p}{dt} = 10(A_p)B - (B_p) \quad (6)$$

Here, A, A_p, Y, Y_p, B and B_p represent, the concentrations of CheA, phosphorylated CheA, CheY, phosphorylated CheY, CheB and phosphorylated CheB, respectively. Li and

392 Hazelbauer (30) have measured the intracellular total concentrations of chemotaxis protein
393 for wild type *E. coli* and are given by, $A + A_p$ = 5.3 µM, $B + B_p$ = 0.28 µM and $Y + Y_p$ = 9.7
394 µM. Note that setting the LHS of equations (2)-(6) equal to zero yields the steady state values
395 of all variables.

396 In order to predict the drift velocity of the cells in gradients of repellent, the
397 clockwise bias (CW bias) was related to CheY-P concentration via a Hill equation (Equation
398 S1), similar to that used by Yuan and Berg (31). The model incorporates the variation of
399 swimming speed, since the swimming speed varied with gradient (Table S1). Note that in
400 case of MeAsp gradients, the swimming speed had remained unchanged (10). The rotational
401 diffusivity (D_r) calculated by Berg (32) for a sphere, 0.062 rad^2/s, was used in the calculation.
402 The distribution of tumble angles is observed to follow a Gamma distribution in agreement
403 with previous studies (Fig. S1)(33). The model also incorporates directional persistence
404 wherein the tumble angle was higher for cells moving down the gradient compared to cells
405 moving in the opposite direction (23). This was achieved by fitting the Gamma distribution
406 function to the measured tumble angle distribution, and using the same for the model
407 calculations (Table S2). The measured tumble angle distribution of cells moving up and down
408 the gradient were used in the model. The details of the swimming speed variation (Table S1),
409 tumble angle distribution (Table S2) along with model equations and numerical
410 implementation are presented in the supplementary information.

411 To explain the observed chemotactic response, we use the above described two-
412 state model to predict the drift velocity for different repellent gradients (See Fig. S2 in
413 Supplementary Information for the algorithm). Although, the swimming speed is a function
414 of the repellent concentration, the swimming speed variation at the three spatial locations
415 (500, 1000, and 1500 µm) for a fixed gradient was less than 10%. Thus the measured average
416 swimming speed of 22.5, 33.9 and 38.8 µm/s was used to predict the drift velocity for

417 gradients of -0.001(10-0), -0.005(50-0), and -0.01(100-0) μM/μm (see Table S1). Further, the
418 measured drift velocity in plain motility buffer and attributed to the cell diffusion and oxygen
419 gradient (1.7 μm/s at 500 μm, 1.1 μm/s at 1000 μm and 0.6 μm/s at 1500 μm) was subtracted
420 from the measured values in repellent gradient for comparison with the model predictions.
421 The predicted values compare well with measurements for all positions along the capillary
422 and for various gradients used in this study (see Fig. 8(A), also Fig. S3 for 100-90 gradient).
423 At short distances from the pellet end ($x=0$), the drift velocities are high due to very low
424 tumble frequency for cells moving down the gradient. As the cells move in the positive x
425 direction, the response to the decreasing concentration increases the tumble frequency
426 thereby reducing the drift velocity. The existing experimental protocol allowed measurement
427 only beyond 500 μm from the pellet thereby missing the initial steep drop in the drift
428 velocity. The values of the parameters used in the model for k, k_1, k_{Ni}, α, β, γ and n are 300,
429 12.75, 300, 0.5, 0.05, 0.065 and 2.2. These parameters are selected to match the measured
430 drift velocity.

431 The mathematical model incorporates the observed increase in swimming speed to
432 predict the drift velocities. Figure 8(B) presents the predicted drift velocity both in the
433 presence and absence of swimming speed enhancement. It is clear that in the absence of the
434 increased swimming speed, the predicted drift velocities are much lower than the observed
435 drift velocity thereby confirming the role of swimming speed variation in the enhancement of
436 drift velocity. Finally, the drift velocity for the mutant strain at the three locations for the 100-
437 0 gradient was identical to that in MB for the same mutant strain, with values of 2.5, 2.1 and
438 1.7 μm/s at distances of 500, 1000, and 1500 μm, respectively, from the cell pellet (data not
439 plotted). Note that the observed drift velocity for the mutant strain is only due to the cell
440 diffusion and oxygen gradient since the sensing mechanism is absent.

441

DISCUSSION

The pioneering work of Tso and Adler (2) established for the first time the negative chemotaxis to various chemicals including metal ions. Using different experimental protocols, they determined the threshold concentration needed for the response. The response in turn was due to the presence of chemoreceptors which senses those particular chemicals. They thus concluded that the harmfulness of a chemical is not responsible for negative chemotaxis. Our work indicates that while the motility of the cells is robust up to 100 µM, the viability of the cells reduces drastically at much higher concentrations. These results are in agreement with those of Englert et al. (5) who found that concentrations lower than 300 µM of $NiSO_4$ had little effect on the aerobic growth of RP437 cells. Tso and Adler (2) reported that the threshold concentration for detecting the Ni^{2+} ions is about 10 µM which is consistent with our observations, since the measured maximum drift velocity for the lowest gradient (10-0) was marginally higher (2 µm/s) than that observed for the motility buffer (1.7 µm/s). Note that the baseline drift velocity observed in motility buffer is due to the cell diffusivity and oxygen effects (10, 11). More recently, Mao et al. (4) used a sophisticated microfluidic set-up to quantify the response of RP437 to varying concentrations of Ni^{2+} ions and they too did not observe a response below 10 µM.

The current understanding of chemotaxis in {\it E. coli} has been obtained via detailed studies of cell motion in response to α-methyl aspartate (MeAsp), a non-metabolizable analogue of Aspartate, and serine which are sensed by the Tar and the Tsr receptors, respectively (34, 35). Most studies have reported constant swimming speeds in gradients of MeAsp (10,33), though recent experiments by Ahmed and Stocker (2008) (36) in steep gradients of MeAsp have shown that the swimming speeds can increase by as much as 30%. Similar response has also been observed in gradients of serine (11,33). Recently, we have demonstrated that the Trg receptor, which senses glucose, plays a role in the variation of

swimming speed even in uniform concentration (zero gradient) of 2-Deoxy-D-glucose (2Dg), a non-metabolizable analogue of glucose (37). The current study demonstrates that swimming speed variation can also occur in the presence of repellents suggesting that as in the case of 2Dg, the increase is due to sensing alone. As was demonstrated in case of the Trg chemoreceptor, in the current study we demonstrated that even the Tar receptor is capable of modulating the swimming speed. Mutant strain devoid of the Tar receptor did not show this effect confirming the role of sensor.

The increased swimming speed can be caused due to faster rotational speed of the flagellar motor that would increase the thrust of the motor thereby leading to higher swimming speeds. The increased speeds may in addition lead to changes in the flagellar bundle geometry such as a better alignment of the bundle along the cell head leading to smoother runs (38). One may therefore speculate that sensing of a repellent leads to a higher flagellar motor speed. To this end, we employed the flickering dark-field microscopy technique to measure the rotation speed of the head, which is a linear function of the flagellar bundle rotation speed (24). In the presence of the repellent gradient, the cell increases its flagellar motor speed leading to much higher swimming speeds compared to that in MB. These changes in either the swimming speed or the head rotation speed were not observed in the mutant strain lacking the Tar receptor. The above results clearly demonstrate, for the first time, a link between sensing and the motor speed. Recently, Demir and Salman (39) have shown that the chemotactic receptor plays a key role in modulating the intra-cellular pH leading to a variation in swimming speed. It is possible that a change in the intra-cellular pH and/or the membrane potential may also occur in response to the repellent to bring about the observed change in swimming speeds though more work is required to confirm this.

A simple model that incorporates receptor dynamics including adaptation, intra-cellular signaling and swimming speed variation was able to qualitatively capture the

observed trend in drift velocity. In absence of the swimming speed variation, the model predicts drift velocities lower than those observed thereby highlighting the relevance of the swimming speed variation. Our studies indicate that the increased swimming speed leads to an enhancement of about 20-40% in the drift velocity over and above that due to modulation of tumble frequency. In conclusion, our studies show that *E. coli* not only modulates the tumble frequency to achieve chemotaxis but the above process may be accompanied by variations in swimming speed leading to an overall enhancement in the drift velocity.

ACKNOWLEDGEMENT

The authors acknowledge financial support from the Department of Science and Technology, India (SB/S3/CE/089/2013) and Department of Biotechnology, India (BT/PR7712/ BRB/10/1229/2013). MST also acknowledges support from the Swaranajayanti Fellowship (DST/SJF/ETA-01/2010-11). Deepti Deepika and Farha Naaz are acknowledged for help with the microchannel experiments.

REFERENCES

1. **Tsang N, MacNab R, Koshland DE Jr.** 1973. Common mechanism for repellents and attractants in bacterial chemotaxis. Science **181**:60-63.
2. **Tso WW, Adler J.** 1974. Negative Chemotaxis in *Escherichia coli*. J Bacteriol. **118**:560- 576.
3. **Imae Y, Oosawa K, Mizuno T, Kihara M, Macnab RM.** 1987. Phenol: a complex chemoeffector in Bacterial chemotaxis. J Bacteriol. **169**:371-379.
4. **Mao H, Cremer PS, Manson MD.** 2003. A sensitive, versatile microfluidic assay for bacterial chemotaxis. Proc Natl Acad Sci USA. **100**:5449-5454.

5. **Englert DL, Manson MD, Jayaraman A.** 2010. A microfluidic device for quantifying bacterial chemotaxis in stable concentration gradients. J Vis Exp. **38**, e1779
6. **Khan S, Trentham DR.** 2004. Biphasic Excitation by Leucine in Escherichia coli Chemotaxis. J Bacteriol. **186**:588-592.
7. **Rosner JL.** 1985. Nonheritable resistance to chloramphenicol and other antibiotics induced by salicylates and other chemotactic repellents in Escherichia coli K12. Proc Natl Acad Sci USA. **82**:8771-8774.
8. **Eisenbach M, Constantinou C, Aloni H, Shinitzky M.** 1990. Repellents for *Escherichia coli* operate neither by changing membrane fluidity nor by being sensed by periplasmic receptors during chemotaxis. J Bacteriol. **172**:5218-5224.
9. **Englert DL,Manson MD, Jayaraman A.** 2010. Repellent Taxis in Response to Nickel Ion Requires neither Ni+2 Transport nor the Periplasmic NikA binding Protein. J Bacteriol. **192**:2633-2637.
10. **Vuppala RV, Tirumkudulu MS, Venkatesh KV.** 2010. Mathematical modeling and experimental validation of chemotaxis under controlled gradients of methyl-aspartate in Escherichia coli. Mol BioSyst. **6**:1082-1092.
11. **Vuppala RV, Tirumkudulu MS, Venkatesh KV.** 2010. Chemotaxis of Escherichia coli to L-serine. Phys Biol. **7**:026007.
12. **Emonet T, Macal CM, North MJ, Wickersham CE, Cluzel P.** 2005. Agent-Cell: a digital single-cell assay for bacterial chemotaxis. Bioinformatics **21**:2714-21.
13. **Morton-Firth CJ, Bray D.** 1998. Predicting temporal fluctuations in an intracellular signalling pathway. J Theor Biol. **192**:117-28.
14. **Morton-Firth CJ, Shimizu TS, Bray D.** 1999. A free-energy-based stochastic simulation of the tar receptor complex. J Mol Biol. **286**:1059-74.

15. **Le Novere N, Shimizu TS.** 2001. STOCHSIM: modelling of stochastic biomolecular processes. Bioinformatics **17**: 575-6.

16. **Bray D, Levin MD, Lipkow K.** 2007. The chemotactic behavior of computer- based surrogate bacteria. Curr Biol **17**: 12-9.

17. **Bray D, Bourret RB, Simon MI.** 1993. Computer simulation of the phosphorylation cascade controlling bacterial chemotaxis. Mol Biol Cell. **4**:469-82.

18. **Bray D, Bourret RB.** 1995. Computer analysis of the binding reactions leading to a transmembrane receptor-linkedmultiprotein complex involved in bacterial chemotaxis. Mol Biol Cell. **6**: 1367-80.

19. **Levin MD, Morton-Firth CJ, Abouhamad WN, Bourret RB, Bray D.** 1998. Origins of individual swimming behavior in bacteria. Biophys J. **74**:175-181.

20. **Manson MD.** 2010. Bacterial chemoreceptors as membrane-spanning allosteric enzymes. Spiro S, Dixon R. SensoryMechanisms in Bacteria: Molecular Aspects of Signal Recognition, Caister Academic Press.

21. **Bapat P, Nandy SK, Wangikar P, Venkatesh KV.** 2006. Quantification of metabolically active biomass using Methylene Blue dye Reduction Test (MBRT):Measurement of CFU in about 200 s. JMicrobiolMethods. **65**:107-116.

22. **Alon U, Camarena L, Surette MG, Arcas BAy, Liu Y, Leibler S, Stock JB.** 1998. Response regulator output in bacterial chemotaxis. EMBO J. **17**:4238-4248.

23. **Saragosti J, Calvez V, Bournaveas N, Perthame B, Buguin A, Silberzan P.** 2011. Directional persistence of chemotactic bacteria in a traveling concentration wave. Proc Natl Acad Sci USA. **108**:16235-16240.

24. **Martinez VA, Schwarz-Linek J, Reufer M, Wilson LG, Morozov AN, Poon WCK.** 2014. Flagellated bacterial motility in polymer solutions. Proc Natl Acad Sci USA. **111**:17771-17776.

25. **Stokes RH, Phang S, Mills R.** 1979. Density, Conductance, Transference Numbers, and Diffusion Measurments in Concentrated solutions of Nickel Chloride a 250 C. J Solution Chem. **8**:489-500.

26. **Englert DL, Manson MD, Jayaraman A.** 2010. Investigation of bacterial chemotaxis in flow-based microfluidic devices. Nat protoc. **5**:864-72.

27. **Boehm A, Kaiser M, Li H, Spangler C, Kasper CA, Ackermann M, Kaever V, Sourjik V, RothV, Jenal U.** 2010. Second messenger mediated adjustment of bacterial swimming velocity. Cell. **141**:107-116.

28. **Silverman M, Simon M.** 1974. Flagellar rotation and the mechanism of bacterial motility. Nature **249**:73-74.

29. **Inoue M, Kaneko K**. 2006. Condition for intracellular adaptive dynamics for chemotaxis. Phys Rev E Stat Nonlin Soft Matter Phys.**74**:011903.

30. **Li M, Hazelbauer GL.** 2004. Cellular Stoichiometry of the Components of the Chemotaxis Signaling Complex. J Bacteriol. **186**:3687-3694.

31. **Yuan J, Berg HC.** 2013. Ultrasensitivty of an adaptive bacterial motor. J Mol Biol. **425**:1760-1764.

32. **Berg HC.** 2010. Random Walks in Biology. Princeton University Press, Princeton.

33. **Berg HC, Brown, DA.** 1972. Chemotaxis in Escherichia coli analysed by three-dimensional tracking. Nature. **239**:502-507.

34. **Eisenbach M.** 2004. Chemotaxis. Imperial college press Chapter 3.

35. **Berg HC.** 2004. *E. coli* in Motion. Springer, New York.

36. **Ahmed T, Stocker R.** 2008. Experimental verification of the behavioral foundation of bacterial transport parameters using microfluidics. Biophys J. **95(9)**:4481-4493.

37. **Deepika D, Karmakar R, Tirumkudulu MS, Venkatesh KV.** 2014. Variation in swimming speed of Escherichia coli in response to attractant. Arch Microbiol. **197(2)**:211-222.

38. **Hyon Y, Marcos, Powers TR, Stocker R, Fu HC.** 2012. The wiggling trajectories of bacteria. J Fluid Mech. **705**:58-76.

39. **Demir M, Salman H.** 2012. Bacterial Thermotaxis by Speed Modulation. Biophysical J. **103**:1683-1690.

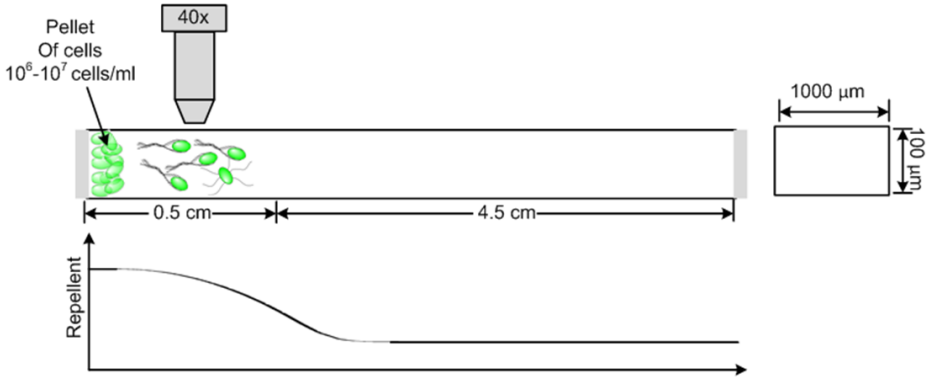

FIG. 1: Experimental setup for establishing gradients of $NiCl_2$ using microchannel. A liquid plug of length 0.5 cm with high concentration of repellent is introduced at the left end of the microchannel while a lower concentration liquid plug of length 4.5 cm in introduced at the right. A concentrated pellet of cells is brought into contact with the repellent at the left end of the microchannel after which the two ends are sealed with wax. Similar experiments using fluorescent metal ion complex of Ni^{2+} was used to obtain the concentration profile in time and space. A schematic of the expected concentration profile is also included.

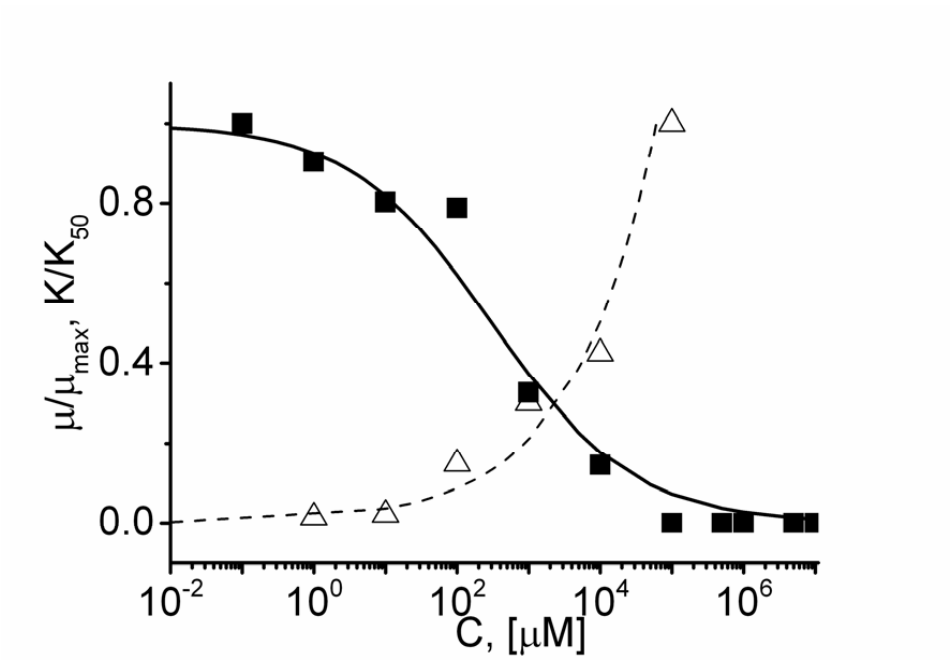

FIG. 2: Normalized specific growth rate, μ/μ_{max} (■), and first order death rate constant, K/K_{50} (Δ), as a function of the repellent concentration for the strain, RP437. The specific growth rate was normalized with the maximum growth rate which was obtained in the absence of any repellent. The death rate constant was normalized with the rate constant observed at 50 *mM* of repellent (K_{50}). Here, $K_{50}=3.47\ h^{-1}$ and $\mu_{max}=0.7\ h^{-1}$. Maximum standard deviation for μ/μ_{max} and K/K_{50} are 0.18 and 0.12 respectively.

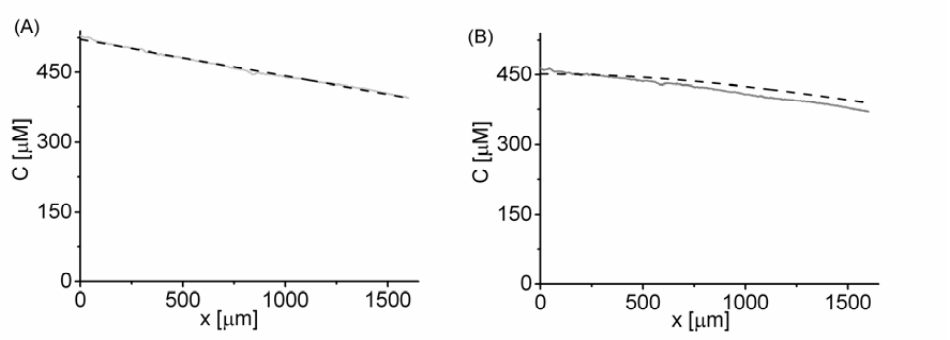

FIG. 3: Concentration profile of the fluorescent metal ion complex in space and time. Concentration at (A) *t=2* min, and (B) *t=25* min. The solid line represents the measurement while the dashed line is the solution of the unsteady state diffusion equation (Equation (1)). The predicted profile was used to obtain the local concentration and the concentration gradient as a function of space and time. The variation in the observed gradient is less than 6% suggesting that the gradient is stable for the entire duration of a typical chemotaxis experiment (less than 25 min).

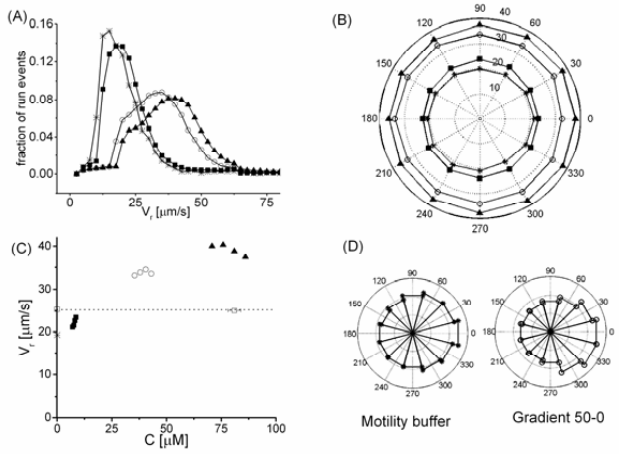

FIG. 4: (A) Distribution of swimming speed for plain motility buffer (i.e. in the absence of repellent, *), and gradients of 10-0 (■), 50-0 (○), and 100-0 (▲) measured at 500 µm from the edge of the pellet. A run event occurs when a cell is in run mode between two subsequent frames (0.047 s apart). The above plot is obtained from more than 10,000 run events for each condition. (B) Angular distribution of the swimming speeds. The numbers along the circumference are angles in degrees while the numbers '20' and '40' in the radial direction are the swimming speeds in µm/s. The swimming speed is isotropic in all cases suggesting that the swimming speed is not a function of the swimming direction. The legend (not included) is the same as that for (A). (C) Mean swimming speed as a function of the repellent concentration. The mean standard error is ± 0.1 µm/s which corresponds to a standard deviation of about 10-14 µm/s. Note that the swimming speed for the lowest gradient (10-0) is close to that in motility buffer (* on ordinate). The legend (not included) is the same as that for (A). The figure also includes the mean speeds measured in motility buffer and gradient of 100-0 for the RP437Δ*tar* strain (□ with dotted line connecting the two points). (D) Angular distribution of the swimming direction for motility buffer (left panel) and, repellent gradient of 50-0 (right panel), both measured at 500 µm from the edge of the pellet. Note that a larger fraction of cells swim down the gradient compared to that in motility buffer.

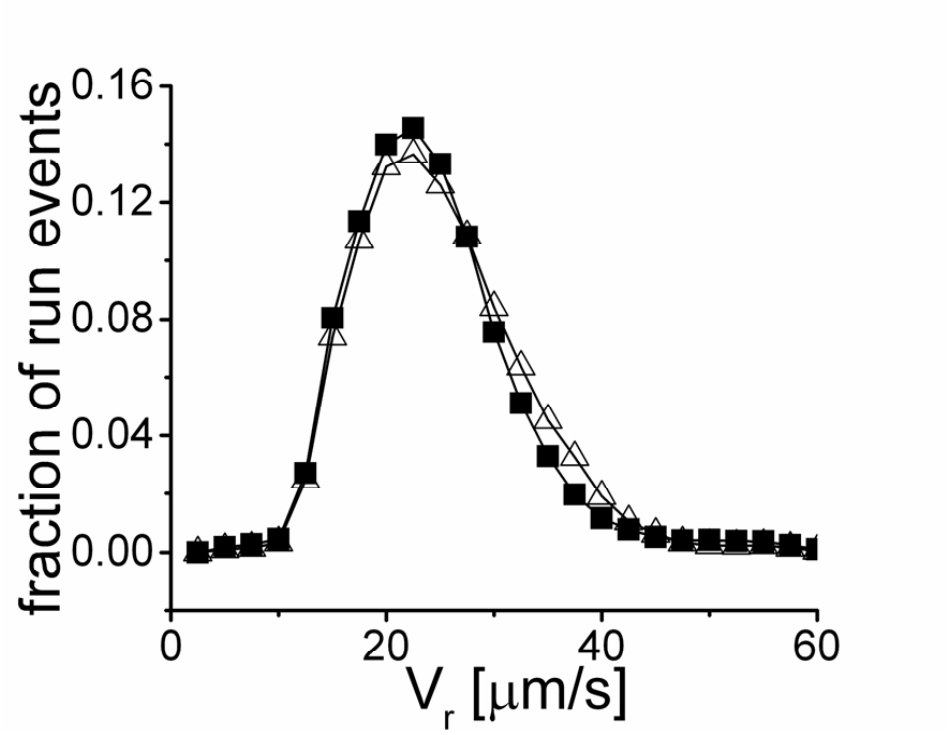

FIG. 5: Distribution of swimming speed for the mutant strain (RP437Δ*tar*) in motility buffer (■) and in gradient of 100-0 (Δ), both measured at 500 μm from the edge of the pellet. A run event occurs when a cell is in run mode between two consequent frames (0.047 s apart). The above plot is obtained from more than 10,000 run events for each condition.

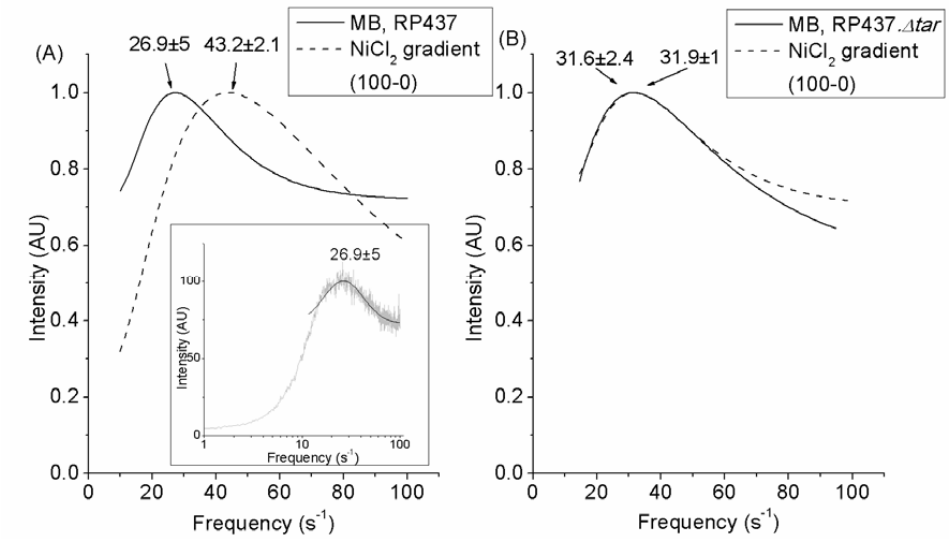

FIG. 6: The power spectrum for (A) wild-type (RP437), and (B) RP437Δ*tar* strains for plug of cells exposed to MB and in a gradient of 100-0 of repellent. In both cases, the measurements were made at 500 µm from the cell pellet. The lines are obtained from a log-normal fit to the averaged data from at least 10 different experiments. The arrows point to the location of the peak in the power spectrum, and the numbers (along with the standard deviation) indicate the peak head-rotation speed. The standard deviation was obtained by determining the peak value for each of the 10 or so experiments and then determining the standard deviation among the peak values. The inset in (A) shows the averaged data for RP437 in MB and the corresponding log-normal fit (black line).

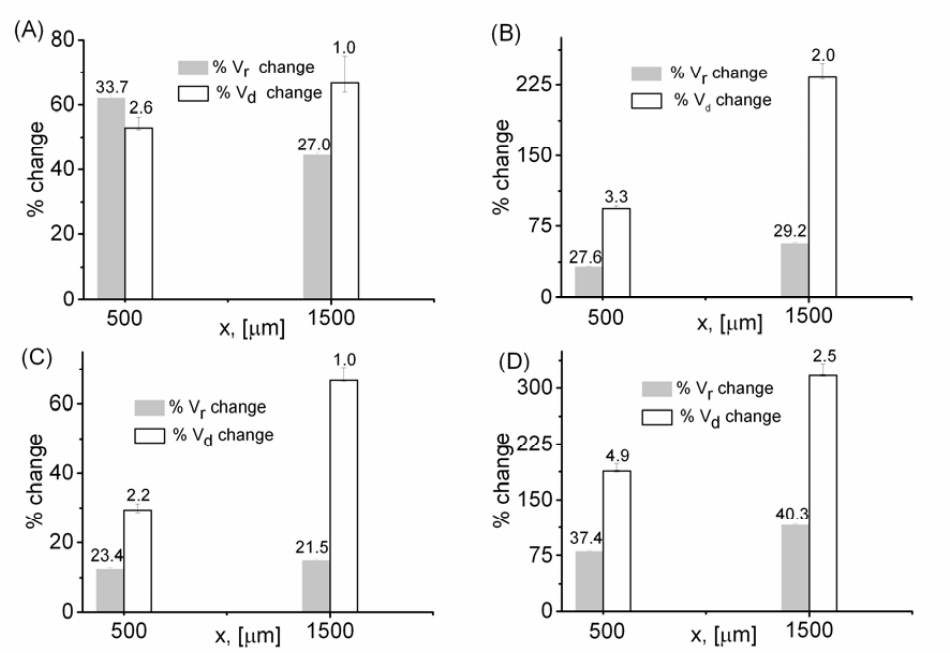

703

704 FIG. 7: Enhancement in swimming speed (gray bar) and drift velocity (empty bar) during
705 (A)100-100 (B)100-90 (C) 10-0 (D) 100-0 repellent gradient relative to the swimming speed
706 and drift velocity in motility buffer. The observed swimming speed in the presence of
707 motility buffer at locations 500 µm and 1500 µm, were 20.8 and 18.7 µm/s respectively,
708 while the corresponding drift velocities were 1.7 and 0.6 µm/s. The measured values of the
709 swimming speed and the drift velocity for each case is included above the corresponding bar.
710 The latter has not been subtracted with the corresponding values measured in MB. The %
711 change is obtained from the ratio of change in swimming speed or drift velocity (with respect
712 to that in MB) to the corresponding value in MB.

713

714

715

716

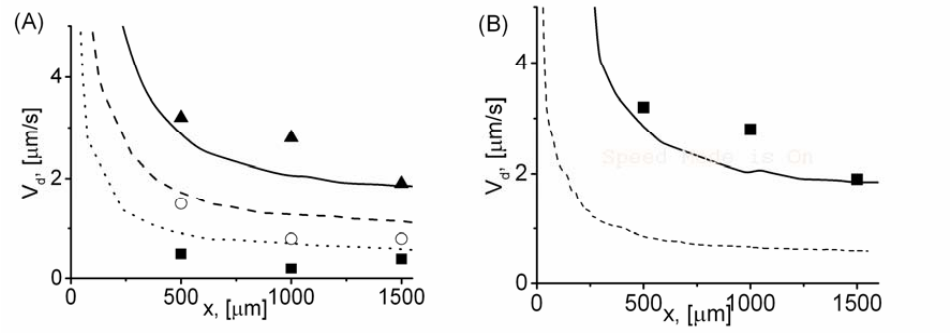

FIG. 8: (A) The spatial variation of the drift velocity for three different gradients of repellent: 10-0(■, dotted line), 50-0 (○, dash line), and 100-0 (▲, solid line). Points are measurements and lines are model prediction. (B) Drift velocity as a function of position in repellent gradient of 100-0. Points are measurements, the solid line is model prediction and the dotted line is the prediction obtained in the absence of swimming speed variation. The drift velocity due to cell diffusion and oxygen gradient has been subtracted in case of measurements. The mean standard error is ± 0.005 μm/s which corresponds to a standard deviation of about 0.2-0.4 μm/s.